Supporting Information

Design and Synthesis of Vanadate-Based Ratiometric Fluorescence Probe for Sequential Recognition of Cu^{2+} and Biothiol

Hui-Hui Zeng,* Zhi-Ying Zhou, Fang Liu, Jie Deng, Shu-Yun Huang, Guo-Ping Li, Pei-Qing Lai, Yue-Ping Xie, Wei Xiao

Jiangxi Key Laboratory of Industrial Ceramics, College of Materials and Chemical Engineering, Pingxiang University, Pingxiang 337055, China

* Corresponding author. Tel: +86 13479865212. E-mail address: zenghuihui1022@163.com

TABLE OF CONTENTS

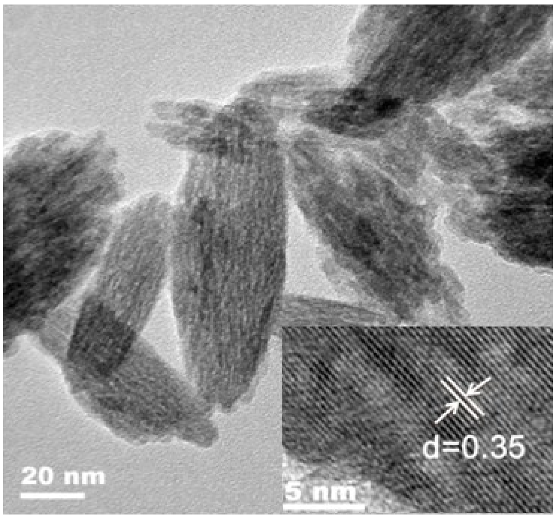

Figure S1 TEM image of $YVO_4:Eu^{3+}$. Insert shows the high-resolution TEM (HRTEM) image of $YVO_4:Eu^{3+}$ (200 crystal plane)

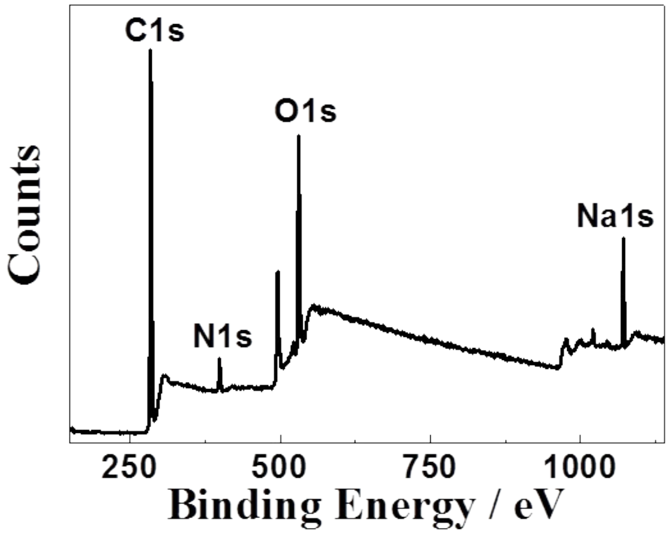

Figure S2 Full range XPS spectra of CDs

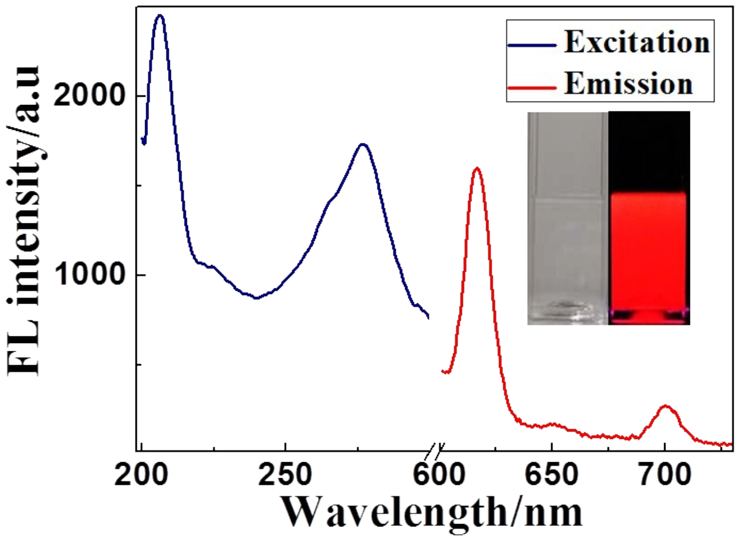

Figure S3 the fluorescence spectrum of $YVO_4:Eu^{3+}$. Inset shows the photograph of $YVO_4:Eu^{3+}$

under daylight (left) and a 254 nm UV lamp (right), respectively.

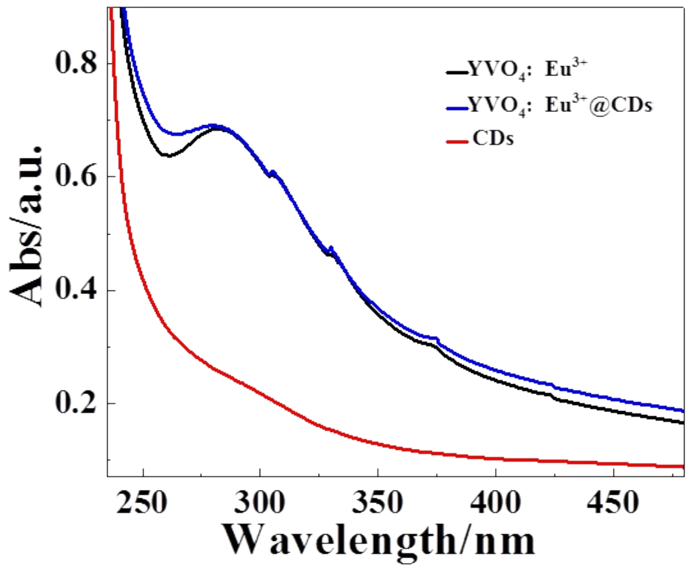

Figure S4 UV-Vis absorption spectra of CDs, $YVO_4:Eu^{3+}$ nanoparticles, and $YVO_4:Eu^{3+}$@CDs

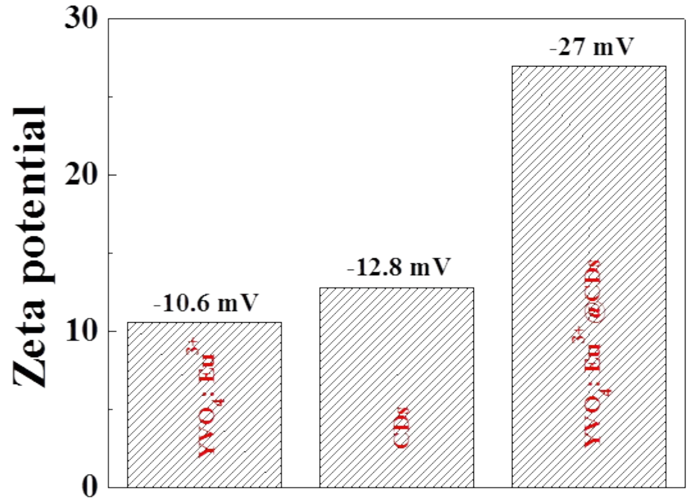

Figure S5 The ζ-potentials of CDs, $YVO_4:Eu^{3+}$, $YVO_4:Eu^{3+}$@CDs

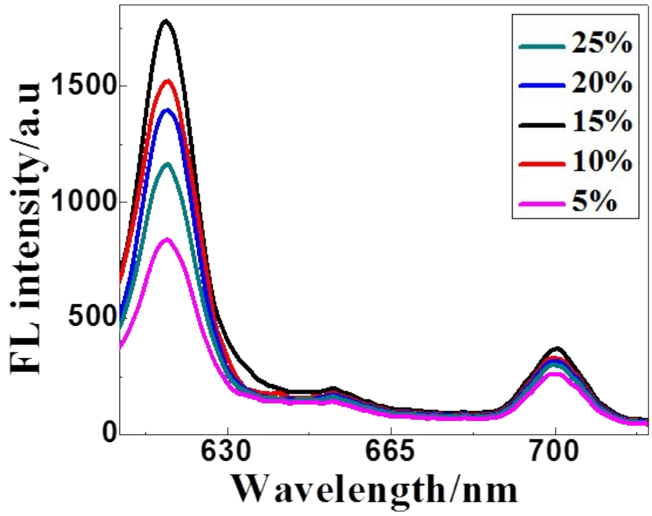

Figure S6 the FL spectrum of YVO_4:Eu^{3+} (0.625 μM) with different doping concentration of Eu^{3+}

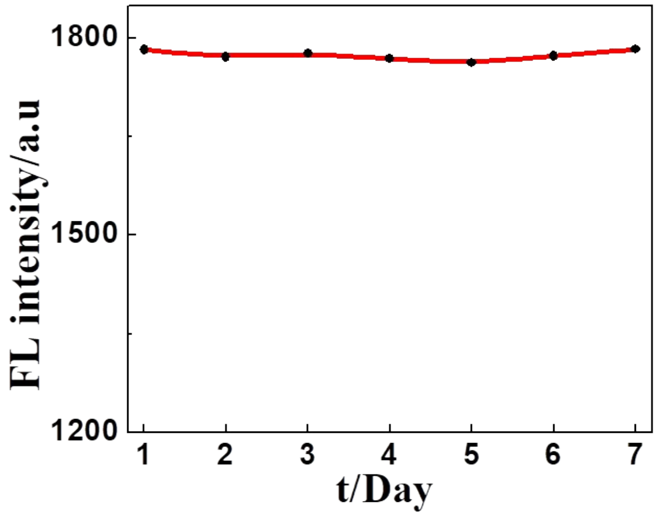

Figure S7 the FL intensity of 617 nm fluorescence peak of YVO_4:Eu^{3+}@CDs (0.625 μM) at different day

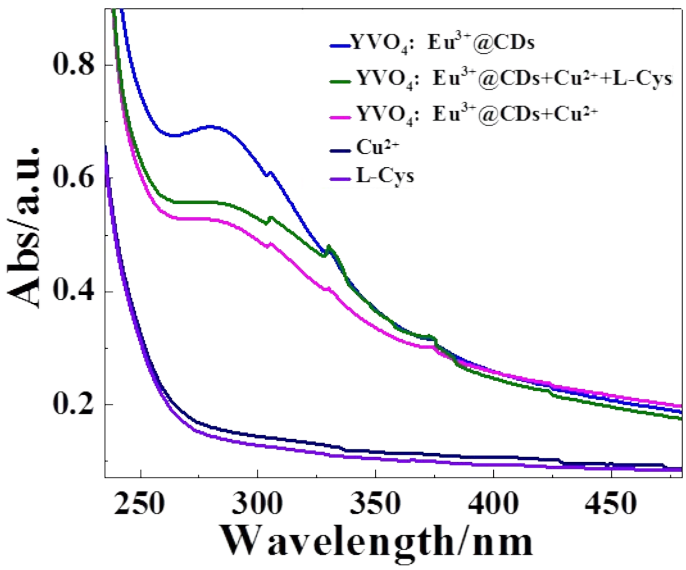

Figure S8 UV-vis absorption spectra of YVO_4:Eu^{3+}@CDs before and after added Cu^{2+} ions and L-Cys

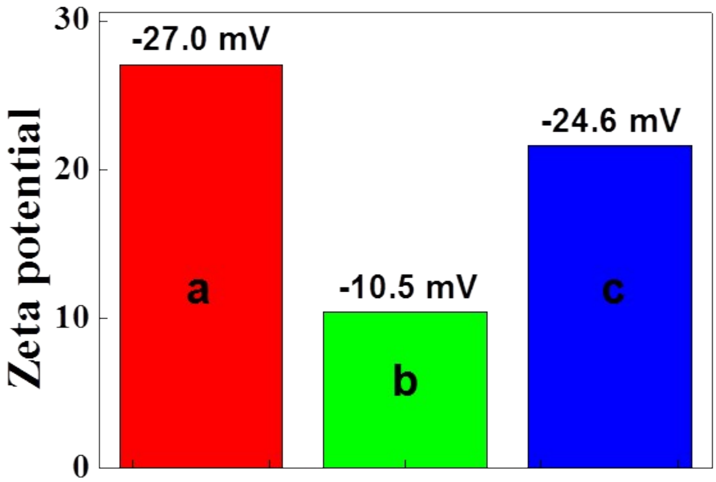

Figure S9 The ζ-potentials of YVO_4:Eu^{3+}@CDs (0.625 μM) (a), YVO_4:Eu^{3+}@CDs added Cu^{2+} (b), YVO_4:Eu^{3+}@CDs added Cu^{2+} and L-Cys (c). The concentration of Cu^{2+} ions and L-Cys is 2 μM,

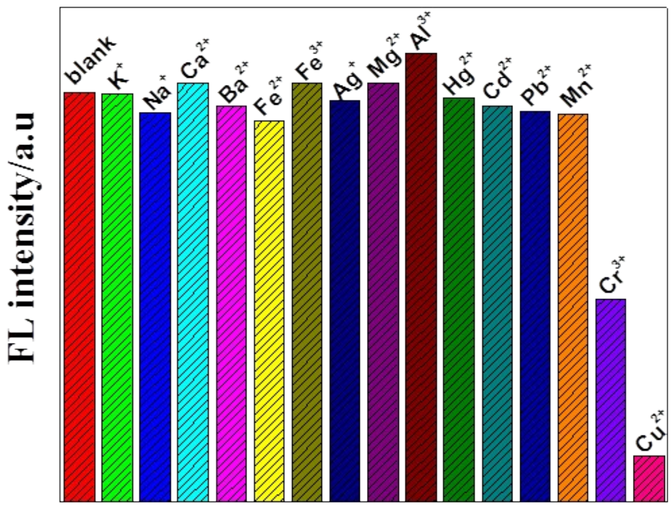

Figure S10 the fluorescence intensity of YVO_4:Eu^{3+}@CDs (0.625 μM) at 617 nm in the presence of different ions. The concentration of all ions is 2μM.

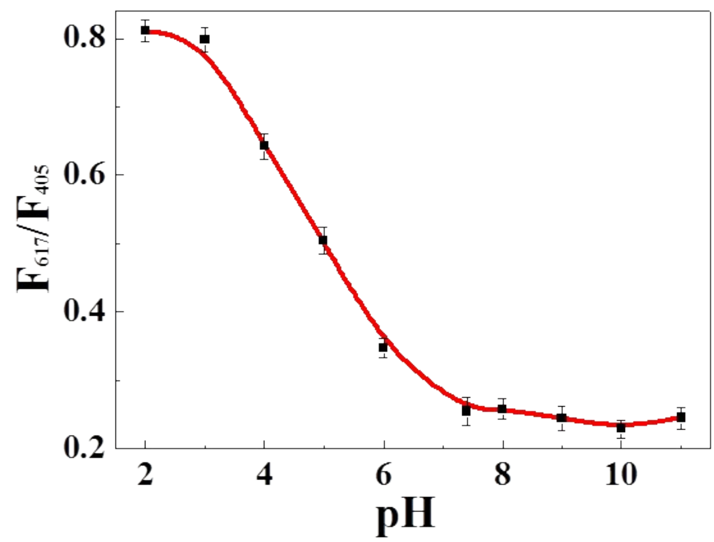

Figure S11 optimization of the pH for Cu^{2+} ions detection, where F_{617} and F_{405} are the FL intensities of $YVO_4:Eu^{3+}$@CDs (0.625 μM) at 617 nm and 405 nm in the presence of Cu^{2+} ions (2 μM)

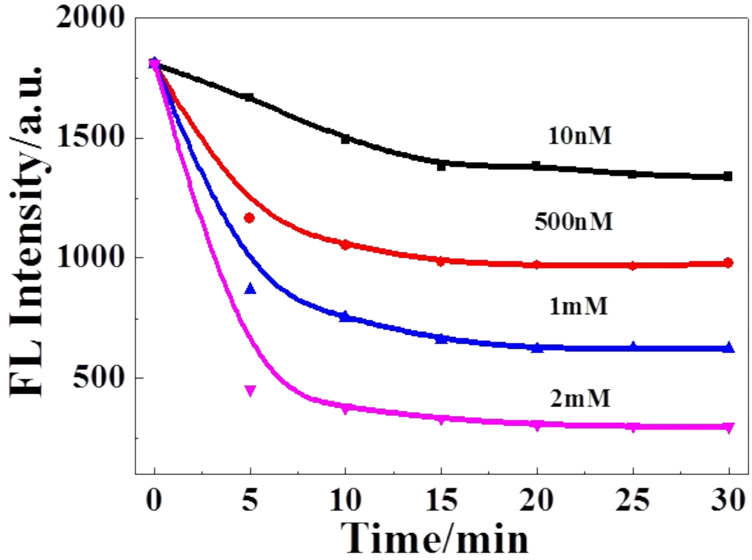

Figure S12 optimization of the time for Cu^{2+} ions detection with the fluorescence intensity of $YVO_4:Eu^{3+}$@CDs (0.625 μM) at 617 nm

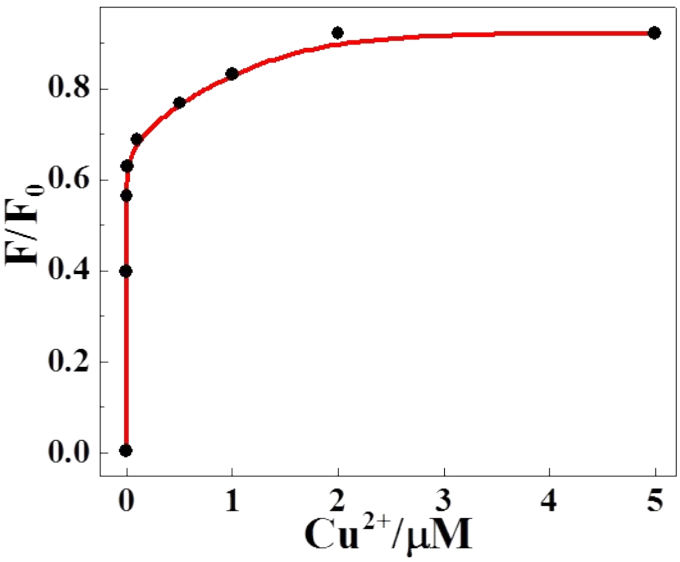

Figure S13 optimization of the concentration of Cu^{2+}. Where F_0 and F are the FL intensities of YVO_4:Eu^{3+}@CDs (0.625 μM) at 617 nm before and after adding Cu^{2+}, respectively.

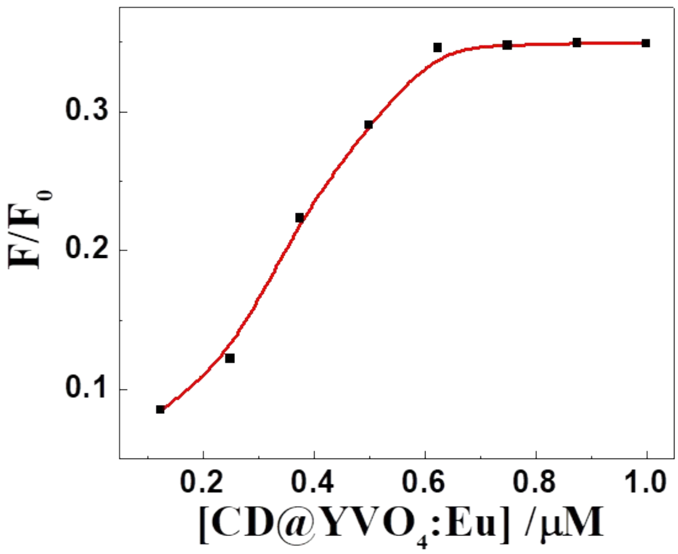

Figure S14 optimization of the concentration of YVO_4:Eu^{3+}@CDs for Cys detection. Where F_0 and F are the FL intensities of YVO_4:Eu^{3+}@CDs at 617 nm before and after adding Cys, respectively

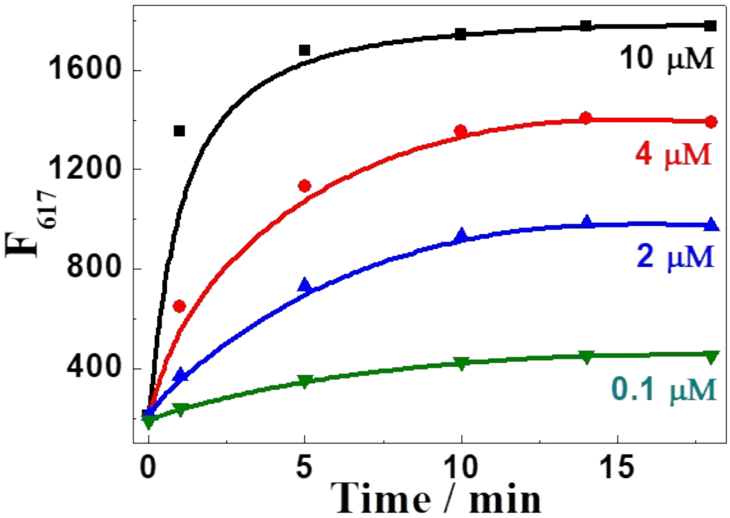

Figure S15 Time-dependent PL responses of $YVO_4:Eu^{3+}$@CDs (0.625 μM) upon addition of different concentrations of Cys, 10 μM (black line), 4 μM (red line), 2 μM (blue line), 0.1 μM (green line).

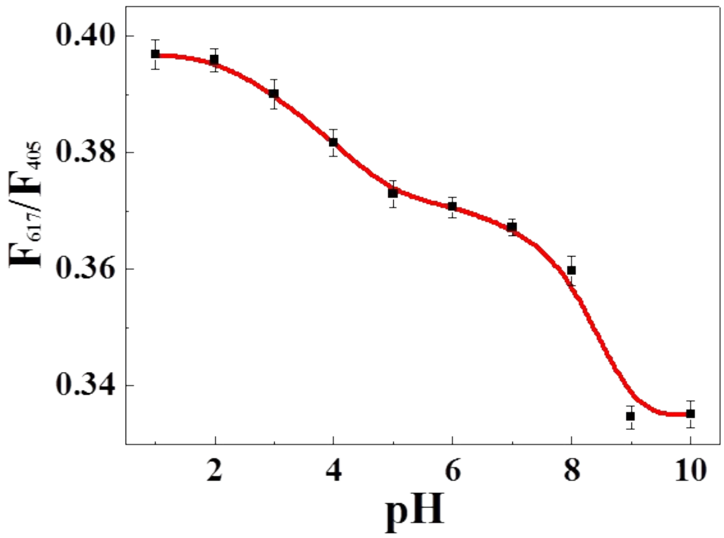

Figure S16 optimization of the pH for L-Cys detection, where F_{617} and F_{405} are the FL intensities of $YVO_4:Eu^{3+}$@CDs (0.625 μM) at 617 nm and 405 nm in the presence of Cu^{2+} ions (2 μM) and L-Cys (2 μM)

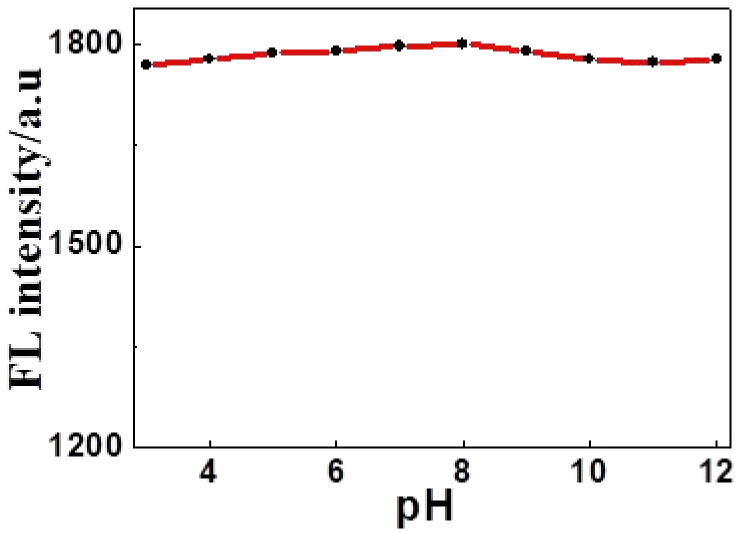

Figure S17 Effect of pH on the FL intensity of 617 nm fluorescence peak of $YVO_4:Eu^{3+}$@CDs (0.625 μM).

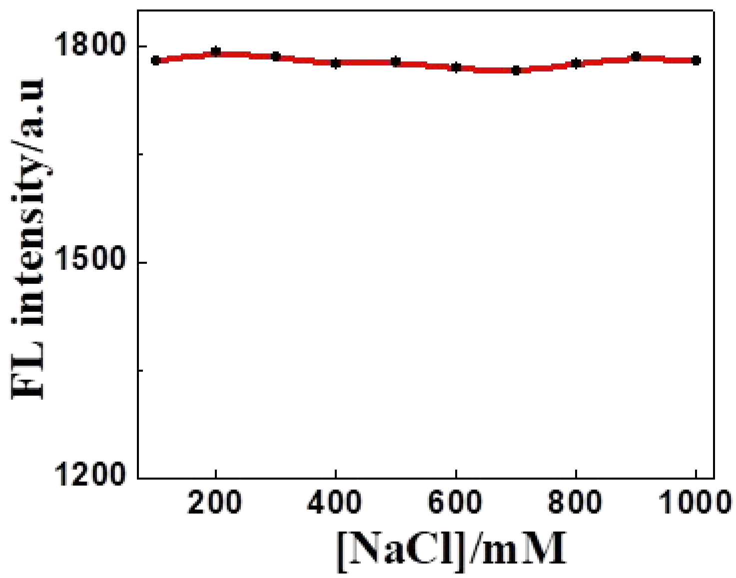

Figure S18 Effect of the concentration of NaCl on the FL intensity of 617 nm fluorescence peak of $YVO_4:Eu^{3+}$@CDs (0.625 μM).

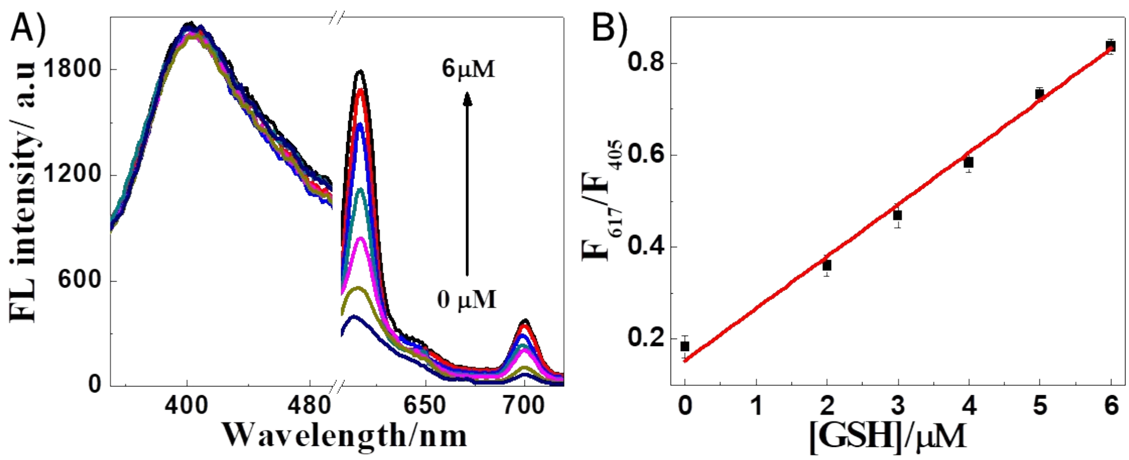

Figure S19 A) the FL spectrum of $YVO_4:Eu^{3+}$@CDs (0.625 μM) at different concentration of GSH. B) Plot of F_{617}/F_{405} against the concentrations of GSH ranging from 0 to 6 μM (where F_{617} and F_{405} are the FL intensities of $YVO_4:Eu^{3+}$@CDs at 617 and 405 nm, respectively).

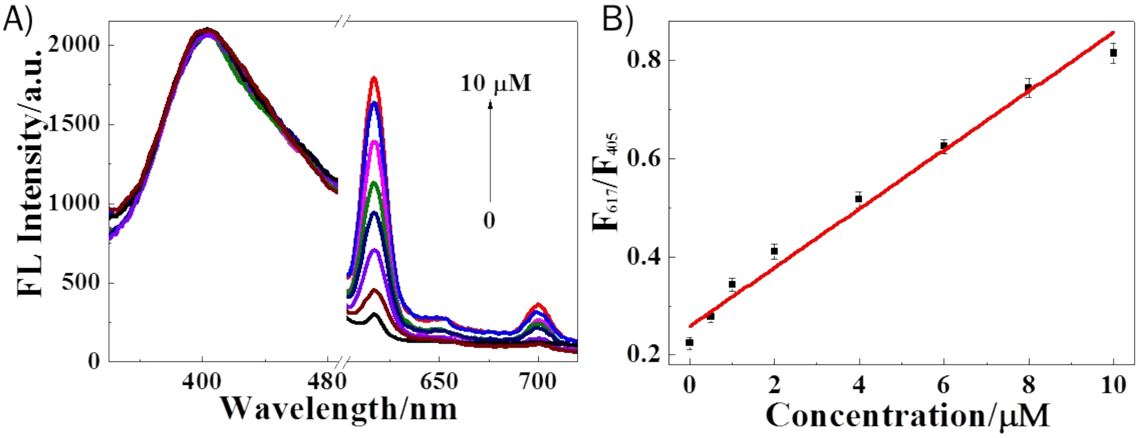

Figure S20 A) the FL spectrum of $YVO_4:Eu^{3+}$@CDs (0.625 μM) at different concentration of Hcy. B) Plot of F_{617}/F_{405} against the concentrations of Hcy ranging from 0 to 6 μM (where F_{617} and F_{405} are the FL intensities of $YVO_4:Eu^{3+}$@CDs at 617 and 405 nm, respectively).

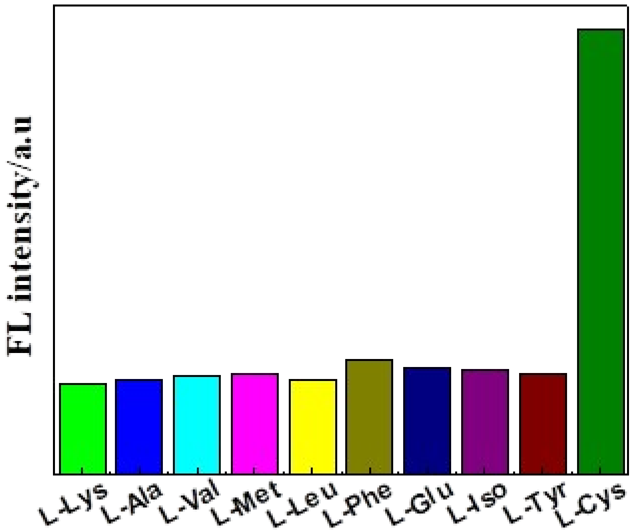

Figure S21 Selectivity competition experiments for $YVO_4:Eu^{3+}$@CDs (0.625 μM) toward different interferences. All amino acid were at a concentration of 10 μM.

Table S1 Comparison of different method for Cu^{2+} ions detection

Analyst method	probe	Linear range (μM)	LOD (μM)	Refer
electrochemical	α-synuclein	—	50 μM	[1]
electrochemical	Cu^{2+}-EDTA chelates	10~1000 μg/L	5.16 nM	[2]
colorimetric	DNA/Au NPs	0.625~15	0.29 μM	[3]
colorimetric	Organic phenol probe	—	4.33 μM	[4]
colorimetric	Ag NPs	0.1~10	0.5 μM	[5]
fluorescence	Ir(III) complexes	0~2.0 eq	2.23×10^{-2} μM	[6]
fluorescence	Au NCs	0~60	0.08 μM	[7]
fluorescence	Graphene QDs	0~15	0.23 μM	[8]
fluorescence	Benzothiazole	—	41.71 nM	[9]
fluorescence	$YVO_4:Eu^{3+}$@CDs	0.001~2	0.2 nM	In this work

Table S2 Comparison of different method for biothiol detection

Analyst method	probe	Linear range (μM)	LOD (μM)	Refer
electrochemical	Au NPs/Bi_4NbO_8Cl	0.1~5	0.01 μM	[10]
colorimetric	Organic phenol probe	—	4.27 μM	[4]
fluorescence	N-GQD	15~125	0.05 μM	[11]
fluorescence	TCF	—	0.28 μM	[12]
fluorescence	Graphene quantum dots	—	0.15 μM	[13]
fluorescence	organic QG-1	—	5.4 mM	[14]
fluorescence	Organic BODYPY dye	—	0.096 μM	[15]
fluorescence	$YVO_4:Eu^{3+}$@CDs	0.2~6	72 nM	In this work

Table S3 Determination of Cu^{2+} ions in human plasma

sample	Added (μM)	Detected [a] (mean, μM)	Recovery [b] (%)	Detected [c] (mean, μM)	RSD (n=3, %)
Plasma 1	0.0	16.250		16.196	2.1
	1.0	17.136	88.6		2.6
	2.0	18.402	107.6		1.0
Plasma 2	0.0	20.124		20.132	2.9
	1.0	21.210	108.6		1.8
	2.0	22.050	96.3		2.2

[a] The measurement results by using the present method

[b] Mean of three determinations.

[c] The measurement results by using the atomic absorption spectrometry method.

Reference

1.S. Li and K. Kerman, Electrochemical Detection of Interaction between Copper(II) and Peptides Related to Pathological α-Synuclein Mutants, *Anal. Chem.*, 2019, **91**, 3818-3826.

2.Q. Shu, M. Liu, H. Ouyang and Z. Fu, Label-free fluorescent immunoassay for Cu^{2+} ion detection based on UV degradation of immunocomplex and metal ion chelates, *Nanoscale*, 2017, **9**, 12302-12306.

3.Y. Wang, F. Yang and X. Yang, Label-free colorimetric biosensing of copper(II) ions with unimolecular self-cleaving deoxyribozymes and unmodified gold nanoparticle probes, *Nanotechnology*, 2010, **21**, 205502.

4.B. Saha, P. Saha, A. Mandal, J. P. Naskar, D. Maiti and S. Chowdhury, Sequential detection of Cu^{2+} and cysteine using an imidazole-based chemosensor in aqueous solution, *J. Chin. Chem. Soc-taip*, 2019, **66**, 506-514.

5.L.-J. Miao, J.-W. Xin, Z.-Y. Shen, Y.-J. Zhang, H.-Y. Wang and A.-G. Wu, Exploring a new rapid colorimetric detection method of Cu^{2+} with high sensitivity and selectivity, *Sensor Actuat B-chem.*, 2013, **176**, 906-912.

6.T. Yu, Y. Wang, Z. Zhu, Y. Li, Y. Zhao, X. Liu and H. Zhang, Two new phosphorescent Ir(III) complexes as efficient selective sensors for the Cu^{2+} ion, *Dyes Pigments*, 2019, **161**, 252-260.

7.H. Ding, C. Liang, K. Sun, H. Wang, J. K. Hiltunen, Z. Chen and J. Shen, Dithiothreitol-capped fluorescent gold nanoclusters: An efficient probe for detection of copper(II) ions in aqueous solution, *Biosens. Bioelectron.*, 2014, **59**, 216-220.

8.F. Wang, Z. Gu, W. Lei, W. Wang, X. Xia and Q. Hao, Graphene quantum dots as a fluorescent sensing platform for highly efficient detection of copper(II) ions, *Sensor Actuat B-chem.*, 2014, **190**, 516-522.

9.X. Tian, Y. Zhao, Y. Li, C. Yang and Z. Zhou, Sensitive and selective ratiometric nanosensors for visual detection of Cu^{2+} based on ions promoted oxidation reaction, *Sensor Actuat B-chem.*, 2017, **247**, 139-145.

10.Y.-F. Ruan, N. Zhang, Y.-C. Zhu, W.-W. Zhao, J.-J. Xu and H.-Y. Chen, Photoelectrochemical Bioanalysis Platform of Gold Nanoparticles Equipped Perovskite Bi_4NbO_8Cl, *Anal. Chem.*, 2017, **89**, 7869-7875.

11. A. B. Ganganboina, A. Dutta Chowdhury and R.-a. Doong, N-Doped Graphene Quantum Dots-Decorated V_2O_5 Nanosheet for Fluorescence Turn Off–On Detection of Cysteine, *ACS Appl. Mater & Inter.*, 2018, **10**, 614-624.

12. Sedgwick, Adam C. Gardiner, Jordan E. Kim, Gyoungmi Yevglevskis, Maksims Lloyd, Matthew D. Jenkins, A. Toby A. Bull, Steven D. Yoon, Juyoung James, Tony D. Long-wavelength TCF-based fluorescence probes for the detection and intracellular imaging of biological thiols, *Chem. Commun.,* 2018, 54, 4786-4789.

13. X. Yan, Y. Song, C. Zhu, J. Song, D. Du, X. Su and Y. Lin, Graphene Quantum Dot–MnO_2 Nanosheet Based Optical Sensing Platform: A Sensitive Fluorescence "Turn Off–On" Nanosensor for Glutathione Detection and Intracellular Imaging, *ACS Appl. Mater & Inter.*, 2016, **8**, 21990-21996.

14. Liu, Z.; Zhou, X.; Miao, Y.; Hu, Y.; Kwon, N.; Wu, X.; Yoon, J., A Reversible Fluorescent Probe for Real-Time Quantitative Monitoring of Cellular Glutathione. *Angew. Chem. Int. Ed.*, **2017**, 56 (21), 5812-5816.

15. Yang, X. F.; Huang, Q.; Zhong, Y.; Li, Z.; Li, H.; Lowry, M.; Escobedo, J. O.; Strongin, R. M., A Dual Emission Fluorescent Probe Enables Simultaneous Detection of Glutathione and

Cysteine/Homocysteine. *Chem. Sci.*, **2014**, 5 (6), 2177-2183.